Photoelectron Spectroscopy of Free Multiply Charged Keggin Anions α-$[PM_{12}O_{40}]^{3-}$ (M = Mo, W) in the Gas Phase

Tom Waters,[†] Xin Huang,[†] Xue-Bin Wang,[†] Hin-Koon Woo,[†] Richard A. J. O'Hair,[‡] Anthony G. Wedd,[‡] and Lai-Sheng Wang*,[†]

Department of Physics, Washington State University, 2710 University Drive, Richland, Washington 99354, Chemical Sciences Division, Pacific Northwest National Laboratory, P.O. Box 999, Richland, Washington 99352, School of Chemistry, The University of Melbourne, Parkville, Victoria, Australia, 3010, and the Bio21 Molecular Science and Biotechnology Institute, 30 Flemington Road, Parkville, Victoria, Australia 3010

Received: June 9, 2006; In Final Form: July 26, 2006

Two polyoxometalate Keggin-type anions, α-$PM_{12}O_{40}^{3-}$ (M = Mo, W), were transferred to the gas phase by electrospray; their electronic structure and stability were probed by photoelectron spectroscopy. These triply charged anions were found to be highly stable in the gas phase with large adiabatic electron detachment energies of 1.7 and 2.1 eV for M = Mo and W, respectively. The magnitude of the repulsive Coulomb barrier was measured as ~3.4 eV for both anions, providing an experimental estimate for the intramolecular Coulomb repulsion present in these highly charged anions. Density functional theory calculations were carried out and compared with the experimental data, providing insight into the electronic structure and valence molecular orbitals of the two Keggin anions. The calculations indicated that the highest occupied molecular orbital and other frontier orbitals for $PM_{12}O_{40}^{3-}$ are localized primarily on the μ_2-oxo bridging ligands of the polyoxometalate framework, consistent with the reactivity on the μ_2-oxo sites observed in solution. It was shown that the HOMO of $PW_{12}O_{40}^{3-}$ is stabilized relative to that of $PMo_{12}O_{40}^{3-}$ by ~0.35 eV. The experimental adiabatic electron detachment energies of $PM_{12}O_{40}^{3-}$ (i.e., the electron affinities of $PM_{12}O_{40}^{2-}$) are combined with recent calculations on the proton affinity of $PM_{12}O_{40}^{3-}$ to yield O−H bond dissociation energies in $PM_{12}O_{39}(OH)^{2-}$ as ~5.1 eV.

Introduction

Polyoxometalate anions are early transition metal oxide clusters (e.g., M = V, Mo, W) that find wide applications in analytical chemistry, biomedicine, and catalysis.[1−3] Their high thermal stability, Brönsted acidity and ability to undergo multiple reversible reductions make them ideal reagents for acid−base chemistry, redox reactions, and bifunctional catalysis. They are soluble in a range of common solvents and can be viewed as "soluble metal oxides". More interestingly, these species provide plausible molecular models for metal oxide surfaces.

Anions of the general formula $XM_{12}O_{40}^{n-}$ (e.g., $X = Si^{IV}$, P^{V}, S^{VI}; $M = Mo^{VI}$, W^{VI}) are known as the Keggin anions and adopt highly symmetric quasi-spherical structures (Figure 1). The clusters are composed of twelve edge- and corner-shared MO_6 pseudo-octahedral units around a central XO_4 tetrahedron (Figure 1). The triply charged anions $PM_{12}O_{40}^{3-}$ (M = Mo, W) contain a central phosphorus(V) heteroatom and are two of the more important examples historically.[1−3] The most common structure observed is the α isomer of T_d point symmetry: three MO_6 units share edges to form an M_3O_{13} "cap" and four caps condense around the central XO_4 tetrahedron (O_c: μ_4-O; Figure 1). The twelve metal atoms are in equivalent environments whereas there are four unique oxygen sites (Figure 1).

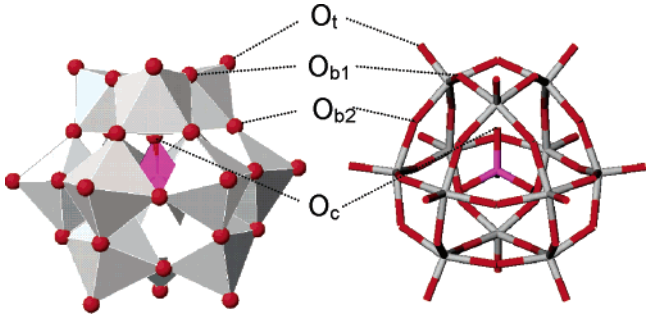

Figure 1. Polyhedral and stick representations of the Keggin anion α-$[PMo_{12}O_{40}]^{3-}$ (molybdenum in gray, oxygen in red, phosphorus in magenta). The four inequivalent oxygen sites are labeled: O_t, terminal; O_{b1}, edge-sharing bridging (μ_2); O_{b2}, corner-sharing bridging (μ_2); and O_c, central (μ_4).

Keggin anions have been the subject of a number of theoretical studies, with the most recent using methods based upon density functional theory (DFT).[4,5] These studies have focused on electronic structure,[6−9] vibrational frequencies,[10,11] the stability of different isomers,[6,12] and acid−base properties.[13−15] Most of these works have assumed isolated $PM_{12}O_{40}^{3-}$ anions.[16,17] However, their fundamental properties in the gas phase as isolated molecular entities have not been explored experimentally, in large part because of difficulties associated with generation of these highly charged anions in the gas phase and uncertainties about their stability due to the anticipated large intramolecular Coulomb repulsion. However, electrospray ionization (ESI) permits transfer of a wide range of solution-phase

* To whom correspondence should be addressed. E-mail: ls.wang@pnl.gov.
[†] Washington State University and Pacific Northwest National Laboratory.
[‡] The University of Melbourne and the Bio21 Institute.

10.1021/jp063594m CCC: $33.50
Published on Web 08/26/2006

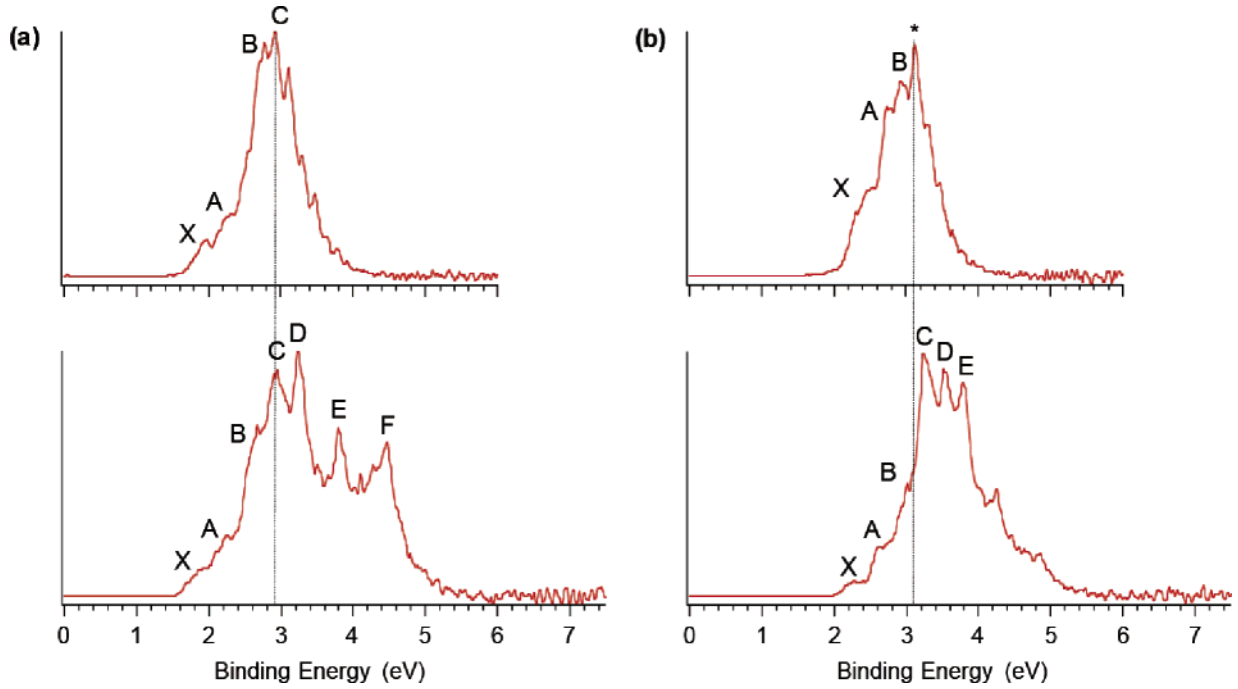

Figure 2. Photoelectron spectra recorded at 157 nm (lower) and 193 nm (upper) of (a) $[PMo_{12}O_{40}]^{3-}$ and (b) $[PW_{12}O_{40}]^{3-}$. The faint vertical line is to guide the eye and relate the position of spectral cutoff in the 193 nm spectrum from the repulsive coulomb barrier to features observed in the 157 nm spectrum.

species into the gas phase and has been applied previously to a number of polyoxometalates including the Keggin anions $[PM_{12}O_{40}]^{3-}$.[18−20] We have studied previously, using ESI, smaller doubly charged oxoanions, such as $M_2O_7^{2-}$ (M = Cr, Mo, W) and $M_6O_{19}^{2-}$ (M = Mo, W).[21,22] Here, we report an experimental and theoretical investigation of the large Keggin anions α-$PM_{12}O_{40}^{3-}$ (M = Mo, W) by a combination of photoelectron spectroscopy (PES) and DFT calculations.

Experimental Details

Photoelectron Spectroscopy. The PES experiments were carried out on a newly built low-temperature instrument that couples an ESI source to a magnetic bottle time-of-flight photoelectron spectrometer.[23,24] The new instrument, which is similar to the one described in detail before,[25] features a cryogenically cooled ion trap, in which anions from the ESI source are stored and collisionally cooled. Briefly, the anions $[PM_{12}O_{40}]^{3-}$ (M = Mo, W) were transferred to the gas phase by electrospray from solutions of $(Bu_4N)_3[PM_{12}O_{40}]$ (M = Mo, W) in CH_3CN (~0.1 mg mL^{-1}). Anions from the ESI source were guided by an RF-only octopole device into a quadrupole mass filter (operated in the RF-only mode in the current experiment), and then guided by a 90° ion bender into the cooled 3D ion trap. The incoming ions were trapped and collisionally cooled by a background gas (~1 mTorr N_2) for a period of 20−100 ms (~(2−10) × 10^3 collisions) to a nominal temperature of about 70 K. The ions were pulsed into the extraction zone of a time-of-flight mass spectrometer at a 10 Hz repetition rate. Ions of interest were mass selected and decelerated before being intercepted by a detachment laser beam (157 nm from an F_2 or 193 nm from an ArF excimer laser) in the interaction zone of the magnetic-bottle photoelectron analyzer. The lasers were operated at a 20 Hz repetition rate with the ion beam off at alternate shots for background subtraction. The photodetached electrons were collected with high efficiency by the magnetic-bottle and analyzed in a 5-meter long electron flight tube. Photoelectron time-of-flight spectra were collected and then converted into kinetic energy spectra, calibrated by the known spectra of $OsCl_6^{2-}$ and I^-.[23−25] Electron binding energy spectra were obtained by subtracting the kinetic energy spectra from the detachment photon energies. Energy resolution ($\Delta E/E$) was estimated to be ~2% (fwhm), i.e., approximately 20 meV for 1 eV electrons, as measured from the spectra of I^- at 355 nm.

Theoretical Calculations. DFT calculations were carried out using the hybrid B3LYP functional[26,27] and the Stuttgart 14-valence electron pseudo-potentials and basis sets for molybdenum and tungsten,[28] and the 6-31+G* basis sets for oxygen and phosphorus.[29,30] Calculations were performed using the NWChem 4.6 program.[31] The geometries of $[PM_{12}O_{40}]^{3-}$ were optimized under T_d symmetry, as observed in the solid state.[32−35] Vertical detachment energies for $PM_{12}O_{40}^{3-}$ were calculated by the ΔSCF method, i.e., the difference in energy between the ground states of the parent $PM_{12}O_{40}^{3-}$ and product $PM_{12}O_{40}^{2-}$ at the geometry of the parent. The energies of the product $PM_{12}O_{40}^{2-}$ were calculated without orbital symmetry constraints to avoid Jahn−Teller problems due to three electrons occupying the doubly degenerate HOMO (formally e under T_d symmetry). Three-dimensional contours of the calculated molecular orbitals were generated using the Extensible Computational Chemistry Environment (Ecce) software.[36]

Experimental Results

Photoelectron spectra of $PM_{12}O_{40}^{3-}$ (M = Mo, W) were recorded at 157 and 193 nm, as presented in Figure 2. The 157 nm spectra exhibit more detachment features due to the higher photon energy, whereas the 193 nm spectra generally exhibit better resolution due to the lower photon energy resulting in lower kinetic energy photoelectrons. The first detachment feature for each species is labeled X, and the remaining ones are labeled A, B, etc. in order of increasing binding energy. Due to the lack of vibrational resolution, the adiabatic detachment energies (ADE's) were measured by drawing a straight line along the leading edge of the threshold band to estimate the onset of the first detachment feature and then adding a constant to correct

for the instrumental resolution and possible thermal broadening. The vertical detachment energies (VDE's) were measured from the peak maximum. Errors were expected to be ±0.1 and ±0.05 eV for the ADE's and VDE's, respectively.

Repulsive Coulomb Barrier. The photoelectron spectra for $PM_{12}O_{40}^{3-}$ are truncated at binding energies below the photon energies due to the repulsive Coulomb barrier (RCB), a general feature for electron detachment from multiply charged anions.[37−41] This barrier to electron detachment arises from the superposition of short range electron attachment and long range Coulomb repulsion between the two negatively charged photoproducts (e.g., $PM_{12}O_{40}^{3-} \rightarrow PM_{12}O_{40}^{2-} + e^-$). The magnitude of the RCB is shown to be equivalent to the intramolecular Coulomb repulsion within a multiply charged anion.[37−41] The RCB manifests itself by preventing photoelectrons of lower kinetic energies (higher binding energies) from leaving the parent anions, resulting in spectral cutoff at the higher binding energy side.

The effect of the RCB is clearly evident in the spectra of $PM_{12}O_{40}^{3-}$ (Figure 2). For example, the features labeled D, E, and F were evident in the 157 nm spectrum of $PMo_{12}O_{40}^{3-}$ in the binding energy range of 3.2−4.5 eV, but not in the 193 nm spectrum, despite the photon energy (6.424 eV) exceeding the binding energies of these features (Figure 2a). Similarly, features C, D, and E were present in the 157 nm spectrum of $PW_{12}O_{40}^{3-}$ in the binding energy range 3.2−3.8 eV but were absent in the 193 nm spectrum (Figure 2b). The magnitude of the RCB can be estimated roughly from the spectral cutoff in the 193 nm spectra for the two $PM_{12}O_{40}^{3-}$ species. Figure 2 shows that the cutoff in the 193 nm spectra for both anions occurs at ∼3 eV, resulting in a RCB of about 3.4 eV for both trianions (photon energy minus the cutoff). The similar RCBs for both $PMo_{12}O_{40}^{3-}$ and $PW_{12}O_{40}^{3-}$ are consistent with their similar sizes and identical ionic charges.

Photoelectron Spectra of $PMo_{12}O_{40}^{3-}$. The first ADE and VDE of $PMo_{12}O_{40}^{3-}$ were measured as 1.7 and 1.94 eV, respectively. The first two features labeled X and A were relatively weak, followed by a number of more intense and closely spaced features at higher binding energies (Figure 2a). Feature B appears as a shoulder on the low binding energy side of feature C in the 157 nm spectrum but is more clearly resolved at 193 nm. Feature C is observed at both 157 and 193 nm, and feature D is partially cut off in the 193 nm spectrum due to the RCB. Features E and F are observed in the 157 nm spectrum but were completely cut off in the 193 nm spectrum by the RCB. Electron detachment beyond ∼4.5 eV in the 157 nm spectrum is prevented by the RCB.

Photoelectron Spectra of $PW_{12}O_{40}^{3-}$. The first ADE and VDE of $PW_{12}O_{40}^{3-}$ were measured as 2.1 and 2.30 eV, respectively, about 0.4 eV higher than that for $PMo_{12}O_{40}^{3-}$. The first two features labeled X and A in the 157 nm spectrum are also relatively weak, similar to the equivalent features for $PMo_{12}O_{40}^{3-}$. These are again followed by a series of closely spaced and more intense features in the 157 nm spectrum. The most intense feature in the 157 nm spectrum, feature C, as well as features D and E, was absent in the 193 nm spectrum due to the RCB. The peak at about 3.1 eV in the 193 nm spectrum (labeled as *) corresponds to the lower binding energy side of feature C but appears as a peak in the 193 nm spectrum due to the effect of cutoff by the RCB. The absence of the most intense feature C in the 193 nm spectrum means that the relative intensity of the weaker features X and A appears higher than in the 157 nm spectrum.

Overall, the PES spectra of the two Keggin anions were rather congested, suggesting that their valence electronic structures are complicated with very closely spaced occupied molecular orbitals. This is understandable, considering the large size of these anions, and is also born out from our DFT calculations described below.

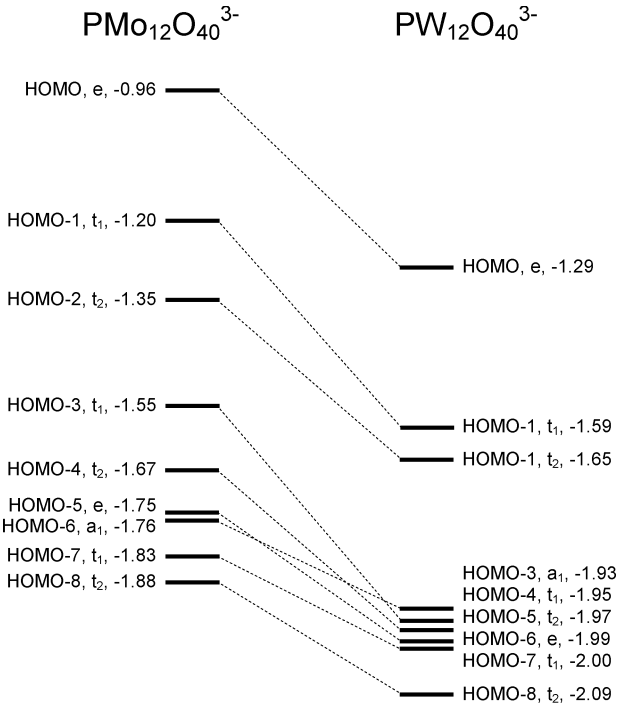

Figure 3. Correlation diagram relating the predicted energies for the nine highest energy occupied orbitals (HOMO to HOMO−8) of $PMo_{12}O_{40}^{3-}$ and $PW_{12}O_{40}^{3-}$. Orbital energies are relative to the vacuum.

Theoretical Results

The geometries of $PMo_{12}O_{40}^{3-}$ and $PW_{12}O_{40}^{3-}$ were optimized under the T_d point symmetry. Calculated bond lengths are in good agreement with experimental values,[32−35] as expected on the basis of recent theoretical studies using similar methodology.[6−11,13] The first VDE's for $PMo_{12}O_{40}^{3-}$ and $PW_{12}O_{40}^{3-}$ were calculated as 1.99 and 2.35 eV, respectively, in very close agreement with the experimental values of 1.94 and 2.30 eV. In particular, the shift of 0.36 eV to higher binding energy from the Mo to W species was accurately reproduced by the calculations.

The calculations predicted an extremely high density of molecular orbitals for about 6 eV below the HOMO, consistent with previous theoretical calculations[8] and the congested PES spectra (Figure 2). A correlation diagram relating the calculated orbital energy levels for the nine highest occupied orbitals (HOMO to HOMO−8) of $PMo_{12}O_{40}^{3-}$ and $PW_{12}O_{40}^{3-}$ is presented in Figure 3. These frontier orbitals are most relevant to the first few detachment features observed experimentally (Figure 2). In general, equivalent orbitals for $PW_{12}O_{40}^{3-}$ were predicted to be stabilized relative to those of $PMo_{12}O_{40}^{3-}$ by about 0.3 eV. In particular, the HOMO of $PW_{12}O_{40}^{3-}$ is stabilized by 0.33 eV, consistent with the VDE of $PW_{12}O_{40}^{3-}$ being 0.36 eV higher than that for $PMo_{12}O_{40}^{3-}$. The doubly degenerate HOMO (of e symmetry) is separated from the HOMO−1 (t_1) by 0.24 and 0.30 eV for $PMo_{12}O_{40}^{3-}$ and $PW_{12}O_{40}^{3-}$, respectively. The HOMO−2 and HOMO−3 levels are predicted to occur at closer energies, whereas the HOMO−3 to HOMO−8 are closely spaced and occur within about 0.3 eV (Figure 3).

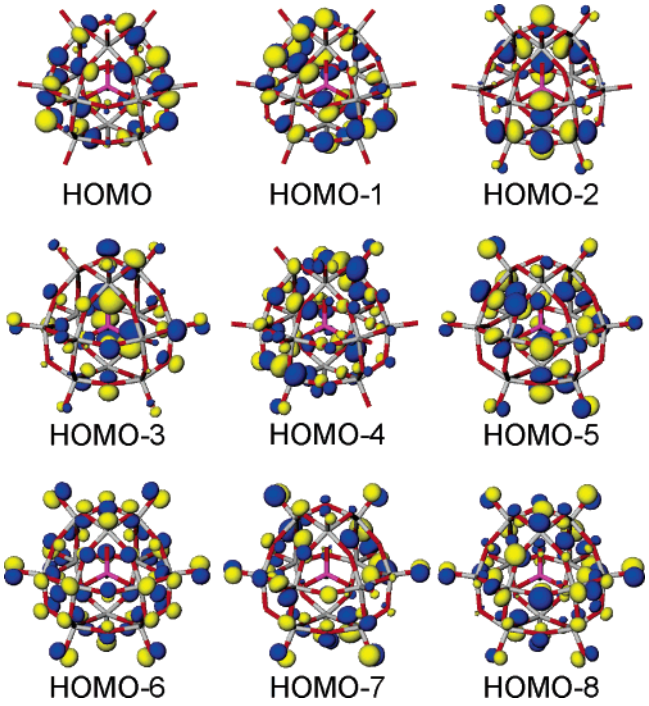

Figure 4. Kohn−Sham molecular orbital contour plots for the nine highest energy occupied frontier orbitals of $PMo_{12}O_{40}^{3-}$.

Kohn−Sham molecular orbital contour plots are presented in Figure 4 for the HOMO to HOMO−8 levels of $PMo_{12}O_{40}^{3-}$. The equivalent orbitals for $PW_{12}O_{40}^{3-}$ are qualitatively very similar, but with some change in ordering (Figure 3). These orbitals are predominantly composed of oxygen 2p lone pairs across the four inequivalent oxygen sites. The HOMO and HOMO−1 levels involve lone pairs on the μ_2-oxo ligands. Similarly, the HOMO−2, HOMO−3, and HOMO−4 levels are localized on μ_2-oxo ligands with a smaller contribution from terminal oxo ligands mixed in. The HOMO−3 also contains a significant contribution from the μ_4-oxo ligands of the central PO_4 unit. The HOMO−5 to HOMO−8 levels contain more significant contributions from the terminal oxo ligands.

Discussion

The photoelectron spectra for $PM_{12}O_{40}^{3-}$ are dominated by broad detachment features, which are expected to arise from the superposition of multiple detachment transitions, as can be seen from the closely spaced molecular orbital energy levels (Figure 3). In addition, most of the frontier orbitals are degenerate, so the first-order Jahn−Teller effect is expected to lead to structural distortions from T_d symmetry in the product $PM_{12}O_{40}^{2-}$, resulting in broad spectral features. The high spectral density and closely spaced molecular orbital energy levels mean that a detailed assignment of the experimentally observed detachment features is not possible. However, the position and intensity of the first few spectral features show qualitative agreement with the molecular orbital energy level scheme of Figure 3.

The HOMO−1 for both of $PM_{12}O_{40}^{3-}$ are predicted to occur about 0.2−0.3 eV below the HOMO, consistent with the experimental separation between features X and A of ∼0.3 eV in both cases. This suggested that feature X should arise from a single detachment transition from the HOMO for both $PM_{12}O_{40}^{3-}$ anions. The width of the X band should be a result of the Jahn-teller effect because of the double degenerate nature of the HOMO.

The HOMO−1 and HOMO−2 levels are predicted to lie between the HOMO and a dense band of orbitals beginning at the HOMO−3. Feature A is likely to arise from detachment from these two orbitals. The HOMO−3 to HOMO−8 levels are predicted to occur at very similar energies, and detachment from these orbitals should contribute to the more intense features B, C, and D; the higher intensity of these features is consistent with the superposition of multiple detachment transitions. As mentioned above, the calculations predicted numerous closely spaced molecular orbitals within ∼6 eV of the HOMO, and features at higher binding energies should arise from the superposition of detachment from these orbitals.

The calculations presented above indicated that the majority of the frontier occupied orbitals of $PM_{12}O_{40}^{3-}$ were localized on the bridging μ_2-oxo ligands, where nucleophilic reactions are known to take place. For example, alkylated derivatives $PM_{12}O_{39}(OCH_3)^{2-}$ have been prepared by electrophilic alkylation of $PM_{12}O_{40}^{3-}$ with the trimethyloxonium ion Me_3O^+. The methyl group is bound to a μ_2-oxo ligand (O_{b1}, Figure 1).[42,43] This is consistent with the frontier orbitals of $PM_{12}O_{40}^{3-}$ being located on the bridging oxo ligands of the Keggin framework, and alkylation at the alternative bridging site (O_{b2}, Figure 1) being disfavored by its lower steric accessibility (Figure 1).[42]

The adiabatic detachment energy of $PM_{12}O_{40}^{3-}$ corresponds to the electron affinity of the doubly charged equivalent $PM_{12}O_{40}^{2-}$. The homolytic O−H bond dissociation energy for $PMo_{12}O_{39}(OH)^{2-}$ (to $PMo_{12}O_{40}^{2-}$ + H) can be estimated from a thermodynamic cycle involving the proton affinity of the parent species (e.g., $PM_{12}O_{39}(OH)^{2-} \rightarrow PM_{12}O_{40}^{3-} + H^+$), the adiabatic electron affinity of the corresponding radical ($PM_{12}O_{40}^{2-} + e^- \rightarrow PM_{12}O_{40}^{3-}$, determined as 1.7 and 2.1 eV for M = Mo, W, respectively, in the present work), and the ionization potential of H (13.60 eV).[44,45] The gas-phase proton affinities of $PMo_{12}O_{40}^{3-}$ have been estimated in recent theoretical studies as 17.1 and 16.6 eV, respectively, for $PMo_{12}O_{40}^{3-}$ and $PW_{12}O_{40}^{3-}$.[13,46] These quantities allow for very similar estimates of ∼5.2 and ∼5.1 eV for the O−H bond dissociation energies in $PMo_{12}O_{39}(OH)^{2-}$ and $PW_{12}O_{39}(OH)^{2-}$, respectively. These values are higher than the C−H bond energy of methane and other hydrocarbons (e.g., CH_4, 4.55 eV),[45] and similar to that estimated for smaller oxometalate anions $MO_2(OH)_2$ (M = Mo, W).[47]

Conclusions

The anions $PMo_{12}O_{40}^{3-}$ and $PW_{12}O_{40}^{3-}$ were transferred to the gas phase using electrospray and their valence electronic structures examined by photodetachment photoelectron spectroscopy. Highly congested photoelectron spectra were observed for both species, consistent with the dense valence molecular orbitals from density functional calculations. Both anions were found to be stable gas-phase species, with adiabatic electron binding energies of 1.7 and 2.1 eV, respectively. The repulsive Coulomb barrier was estimated as ∼3.4 eV for both species, providing an approximate magnitude for the intramolecular Coulomb repulsion in these species. Vertical electron detachment energies calculated using density functional theory were in good agreement with the experimental data. The theoretical calculations showed that the frontier orbitals of $PM_{12}O_{40}^{3-}$ were located on bridging oxo ligands, consistent with their nucleophillic reactivity at these sites. Experimental and theoretical data indicated that the HOMO of $PW_{12}O_{40}^{3-}$ is stabilized relative to that of $PMo_{12}O_{40}^{3-}$ by ∼0.35 eV. The adiabatic electron detachment energies of $PM_{12}O_{40}^{3-}$ (electron affinities of $PM_{12}O_{40}^{2-}$) were combined with recent theoretical calculations

on the proton affinity of $PM_{12}O_{40}^{3-}$ to estimate the O−H bond dissociation energy in $PM_{12}O_{39}(OH)^{2-}$ as ~5.1 eV. These Keggin anions both have molecular dimensions larger than 1 nm; and the current study suggests that it is feasible to probe the electronic structures of individual nanoparticles in the gas phase using ESI and PES.

Acknowledgment. This work was supported by the Chemical Sciences, Geosciences and Biosciences Division, Office of Basic Energy Sciences, U.S. Department of Energy (DOE), under grant No. DE-FG02-03ER15481 (catalysis center program) and was performed at the W. R. Wiley Environmental Molecular Sciences Laboratory (EMSL), a national scientific user facility sponsored by DOE's Office of Biological and Environmental Research and located at Pacific Northwest National Laboratory, operated for DOE by Battelle. Calculations were performed on the EMSL Molecular Science Computing Facility.

References and Notes

(1) (a) Pope, M. T. *Heteropoly and Isopoly Oxometalates*; Springer-Verlag: Berlin, 1983; 180 pp. (b) *Polyoxometalates: from platonic solids to anti retroviral activity*; Müller, A., Pope, M. T., Eds.; Kluwer Academic Publishers: Boston, 1994; 411 pp. (c) *Polyoxometalate Chemistry from Topology via Self-Assembly to Applications*; Pope, M. T., Müller, A., Eds.; Kluwer Academic Publishers: Netherlands, 2001; 467 pp.

(2) Thematic Issue on Polyoxometalates. Hill, C. L., Ed. *Chem. Rev.* **1998**, *98*, No. 1.

(3) Pope, M. T. Polyoxo Anions: Synthesis and Structure. In *Comprehensive Coordination Chemistry II*; McLeverty J. A., Meyer, T. J., Eds.; *Transition Metal Groups 3−6*, Vol. 4; Wedd, A. G., Vol. Ed.; Elsevier: Amsterdam, 2004; pp 635−678.

(4) Rohmer, M. M.; Benard, M.; Blaudeau, J. P.; Maestre, J. M.; Poblet, J. M. *Coord. Chem. Rev.* **1998**, *180*, 1019.

(5) Poblet, J. M.; Lopez, X.; Bo, C. *Chem. Soc. Rev.* **2003**, *32*, 297.

(6) Lopez, X.; Maestre, J. M.; Bo, C.; Poblet, J. M. *J. Am. Chem. Soc.* **2001**, *123*, 9571.

(7) Maestre, J. M.; Lopez, X.; Bo, C.; Poblet, J. M.; Casan-Pastor, N. *J. Am. Chem. Soc.* **2001**, *123*, 3749.

(8) Bridgeman, A. J.; Cavigliasso, G. *J. Phys. Chem. A* **2003**, *107*, 6613.

(9) Guo, Y. R.; Qing-Jiang, P.; Wei, Y. D.; Li, Z. H.; Xin, L. *J. Mol. Struct. (THEOCHEM)* **2004**, *676*, 55.

(10) Bridgeman, A. J. *Chem. Phys.* **2003**, *287*, 55.

(11) Bridgeman, A. J. *Chem.—Eur. J.* **2004**, *10*, 2935.

(12) Lopez, X.; Poblet, J. M. *Inorg. Chem.* **2004**, *43*, 6863.

(13) Ganapathy, S.; Fournier, M.; Paul, J. F.; Delevoye, L.; Guelton, M.; Amoureux, J. P. *J. Am. Chem. Soc.* **2002**, *124*, 7821.

(14) Janik, M. J.; Campbell, K. A.; Bardin, B. B.; Davis, R. J.; Neurock, M. *Appl. Catal., A* **2003**, *256*, 51.

(15) Janik, M. J.; Davis, R. J.; Neurock, M. *J. Am. Chem. Soc.* **2005**, *127*, 5238.

(16) Lopez, X.; Fernandez, J. A.; Romo, S.; Paul, J. F.; Kazansky, L.; Poblet, J. M. *J. Comput. Chem.* **2004**, *25*, 1542.

(17) Lopez, X.; Nieto-Draghi, C.; Bo, C.; Avalos, J. B.; Poblet, J. M. *J. Phys. Chem. A* **2005**, *109*, 1216.

(18) Colton, R.; Traeger, J. C. *Inorg. Chim. Acta* **1992**, *201*, 153.

(19) Tuoi, J. L.; Muller, E. *Rapid Commun. Mass Spectrom.* **1994**, *8*, 692.

(20) Lau, T. C.; Wang, J.; Guevremont, R.; Siu, K. W. M. *Chem. Commun.* **1995**, 877.

(21) Zhai, H. J.; Huang, X.; Waters, T.; Wang, X. B.; O'Hair, R. A. J.; Wedd, A. G.; Wang, L. S. *J. Phys. Chem. A* **2005**, *109*, 10512.

(22) Yang, X.; Waters, T.; Wang, X. B.; O'Hair, R. A. J.; Wedd, A. G.; Li, J.; Dixon, D. A.; Wang, L. S. *J. Phys. Chem. A* **2004**, *108*, 10089.

(23) Wang, X. B.; Woo, H. K.; Kiran, B.; Wang, L. S. *Angew. Chem., Int. Ed.* **2005**, *44*, 4968.

(24) Wang, X. B.; Woo, H. K.; Wang, L. S. *J. Chem. Phys.* **2005**, *123*, 051106.

(25) Wang, L. S.; Ding, C. F.; Wang, X. B.; Barlow, S. E. *Rev. Sci. Instrum.* **1999**, *70*, 1957.

(26) Becke, A. D. *J. Chem. Phys.* **1993**, *98*, 5648.

(27) Lee, C. T.; Yang, W. T.; Parr, R. G. *Phys. Rev. B* **1988**, *37*, 785.

(28) Andrae, D.; Haussermann, U.; Dolg, M.; Stoll, H.; Preuss, H. *Theor. Chim. Acta* **1990**, *77*, 123.

(29) Hehre, W. J.; Ditchfield, R.; Pople, J. A. *J. Chem. Phys.* **1972**, *56*, 2257.

(30) Francl, M. M.; Pietro, W. J.; Hehre, W. J.; Binkley, J. S.; Gordon, M. S.; Defrees, D. J.; Pople, J. A. *J. Chem. Phys.* **1982**, *77*, 3654.

(31) (a) Aprà, E.; Windus, T. L.; Straatsma, T. P.; Bylaska, E. J.; de Jong, W.; Hirata, S.; Valiev, M.; Hackler, M.; Pollack, L.; Kowalski, K.; Harrison, R.; Dupuis, M.; Smith, D. M. A.; Nieplocha, J.; Tipparaju, V.; Krishnan, M.; Auer, A. A.; Brown, E.; Cisneros, G.; Fann, G.; Früchtl, H.; Garza, J.; Hirao, K.; Kendall, R.; Nichols, J.; Tsemekhman, K.; Wolinski, K.; Anchell, J.; Bernholdt, D.; Borowski, P.; Clark, T.; Clerc, D.; Dachsel, H.; Deegan, M.; Dyall, K.; Elwood, D.; Glendening, E.; Gutowski, M.; Hess, A.; Jaffe, J.; Johnson, B.; Ju, J.; Kobayashi, R.; Kutteh, R.; Lin, Z.; Littlefield, R.; Long, X.; Meng, B.; Nakajima, T.; Niu, S.; Rosing, M.; Sandrone, G.; Stave, M.; Taylor, H.; Thomas, G.; van Lenthe, J.; Wong, A.; Zhang, Z. *NWChem, A Computational Chemistry Package for Parallel Computers, Version 4.6*; Pacific Northwest National Laboratory: Richland, WA 99352-0999, 2004. (b) High Performance Computational Chemistry: an Overview of NWChem a Distributed Parallel Application. Kendall, R. A.; Aprà, E.; Bernholdt, D. E.; Bylaska, E. J.; Dupuis, M.; Fann, G. I.; Harrison, R. J.; Ju, J.; Nichols, J. A.; Nieplocha, J.; Straatsma, T. P.; Windus, T. L.; Wong, A. T. *Comput. Phys. Commun.* **2000**, *128*, 260.

(32) Ugalde, M.; Gutierrez-Zorrilla, J. M.; Vitoria, P.; Luque, A.; Wery, A. S. J.; Roman, P. *Chem. Mater.* **1997**, *9*, 2869.

(33) Bi, L. H.; Wang, E. B.; Xu, L.; Huang, R. D. *Inorg. Chim. Acta* **2000**, *305*, 163.

(34) Brown, G. M.; Noespirlet, M. R.; Busing, W. R.; Levy, H. A. *Acta Crystallogr. B* **1977**, *33*, 1038.

(35) You, W. S.; Wang, E. B.; Zhang, H.; Xu, L.; Wang, Y. B. *J. Mol. Struct.* **2000**, *554*, 141.

(36) Black, G.; Didier, B.; Elsethagen, T.; Feller, D.; Gracio, D.; Hackler, M.; Havre, S.; Jones, D.; Jurrus, E.; Keller, T.; Lansing, C.; Matsumoto, S.; Palmer, B.; Peterson, M.; Schuchardt, K.; Stephan, E.; Taylor, H.; Thomas, G.; Vorpagel, E.; Windus, T.; Winters, C. *Ecce, A Problem Solving Environment for Computational Chemistry, Software, Version 3.2.2*; Pacific Northwest National Laboratory: Richland, WA 99352-0999, 2005.

(37) Wang, L. S.; Ding, C. F.; Wang, X. B.; Nicholas, J. B. *Phys. Rev. Lett.* **1998**, *81*, 2667.

(38) Wang, X. B.; Ding, C. F.; Wang, L. S. *Phys. Rev. Lett.* **1998**, *81*, 3351.

(39) Wang, X. B.; Wang, L. S. *Nature* **1999**, *400*, 245.

(40) Wang, L. S.; Wang, X. B. *J. Phys. Chem. A* **2000**, *104*, 1978.

(41) Dreuw, A.; Cederbaum, L. S. *Chem. Rev.* **2002**, *102*, 181.

(42) Knoth, W. H.; Harlow, R. L. *J. Am. Chem. Soc.* **1981**, *103*, 4265.

(43) Knoth, W. H.; Farlee, R. D. *Inorg. Chem.* **1984**, *23*, 4765.

(44) http://webbook.nist.gov/chemistry/.

(45) Blanksby, S. J.; Ellison, G. B. *Acc. Chem. Res.* **2003**, *36*, 255.

(46) Values for the proton affinity at the different bridging oxo sites O_{b1} and O_{b2} were reported as 17.2 and 17.0 eV for $PMo_{12}O_{40}^{3-}$ and 16.5 and 16.7 eV for $PW_{12}O_{40}^{3-}$ in ref 13. We have used the average values of 17.1 and 16.6 eV, respectively, in these calculations.

(47) Waters, T.; Wang, X. B.; Li, S.; Kiran, B.; Dixon, D. A.; Wang, L. S. *J. Phys. Chem. A* **2005**, *109*, 11771.